Experimental observation of a symmetry-protected bound state in the continuum in a chain of dielectric disks

Z. F. Sadrieva,[1] M. A. Belyakov,[1] M. A. Balezin,[1] P. V. Kapitanova,[1] E. A. Nenasheva,[2] A. F. Sadreev,[3] and A. A. Bogdanov[1,4,*]

[1]*Department of Nanophotonics and Metamaterials, ITMO University, St. Petersburg 197101, Russia*
[2]*Giricond Research Institute Ceramics Co. Ltd., St. Petersburg 194223, Russia*
[3]*Kirensky Institute of Physics Federal Research Center, KSC SB RAS, 660036 Krasnoyarsk, Russia*
[4]*Ioffe Institute, St. Petersburg 194021, Russia*

(Received 3 June 2018; revised manuscript received 5 January 2019; published 2 May 2019)

The existence of bound states in the continuum (BIC) manifests a general wave phenomenon first predicted in quantum mechanics by John von Neumann and Eugene Wigner [J. von Neumann and E. Wigner, Phys. Z. 30, 465 (1929)]. Today it is being actively explored in photonics, radiophysics, acoustics, and hydrodynamics. We report an experimental observation of an electromagnetic bound state in the radiation continuum in a one-dimensional array of dielectric particles. By measurement of the transmission spectra of the ceramic disk chain at GHz frequencies, we demonstrate how a resonant state in the vicinity of the center of the Brillouin zone turns into a symmetry-protected BIC with increase in the number of the disks. We estimate a number of the disks when the radiation losses become negligible in comparison to material absorption and, therefore, the chain could be considered practically as infinite. The presented analysis is supplemented by measurements of the near fields of the symmetry-protected BIC. All measurements are in a good agreement with the results of the numerical simulation and analytical model based on a tight-binding approximation. The obtained results provide useful guidelines for practical implementations of structures with bound states in the continuum that opens up horizons for the development of optical and radio-frequency metadevices.

DOI: 10.1103/PhysRevA.99.053804

I. INTRODUCTION

It is well known that a dielectric rod or slab supports waveguide modes formed under the condition of total internal reflection from the waveguide boundaries [1]. The wave numbers of the waveguide modes lie under the light line of the surrounding space making them orthogonal to the radiation continuum. When the dispersion curve crosses the frequency cutoff, the waveguide mode turns into a leaky mode (resonant state) [1]. However, recently it was acknowledged that the introduction of periodic modulation of the refractive index along the axis of the rod or slab discretizes the radiation continuum, and this could result in complete suppression of radiation losses for leaky modes [2–7]. Therefore, the resonant state becomes localized, i.e., totally decoupled from the radiation continuum. Such localized solutions are known as *bound states in the continuum* (BICs) [8,9]. Recently, the immense progress in handling photonic crystals has encouraged extensive studies on BICs in various periodic photonic structures [5,10–29]. These studies are predominantly motivated by potential applications in resonant enhancement [30–33], lasing [34,35], filtering of light [36,37], biosensing [38,39], encasement of light-matter coupling [40], and polarization control [41,42]. The mechanism resulting in the appearance of BIC in periodic structures results in the appearance of high-Q states (*quasi-BIC*) in single resonators [43–47].

Among the variety of the considered designs of photonic structures, the one-dimensional arrays of spheres or disks are distinctive because of the rotational symmetry. It gives rise to the existence of BICs with orbital angular momentum. In the scattered spectra, such a state manifests itself as a scattered field with orbital angular momentum traveling along the array [5,7,21,48]. This could be used for the generation of *twisted light* and, therefore, for optomechanical manipulations [49], quantum cryptography, and other applications [2,50]. The theory of BICs in the one-dimensional arrays of spheres and disks is developed in Refs. [6,51] but, in spite of a variety of potential applications, experimental study has not been presented to date.

In this work, we report an experimental study of BICs in a one-dimensional (1D) axially symmetric array of dielectric particles. We study the transformation of the resonant state into symmetry-protected BIC with an increase of the number of the scatterers by measurement of the transmission characteristic of the chain. In order to make the analysis more reliable, we measure the field profiles, which confirm observation of the symmetry-protected BIC.

II. THE RESONANT STATES IN PERIODIC ARRAY OF DIELECTRIC DISKS

A. General theory of BIC in 1D chain

The basic theory of BICs in the periodic stack of an infinite number of dielectric disks is presented in Ref. [51]. Here, we briefly give the fundamentals of BIC theory and introduce the basic notations used further. According to the Bloch theorem,

*Corresponding author: a.bogdanov@metalab.ifmo.ru

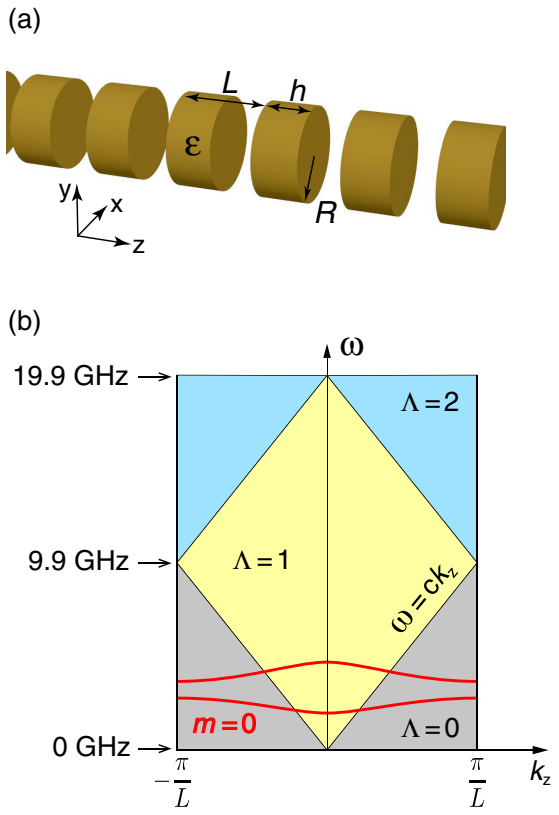

FIG. 1. (a) Chain of ceramic disks with $\varepsilon = 40$, radius $R = 10.2$ mm, and thickness $h = 10.1$ mm arranged in an array with period $L = 15.1$ mm. (b) Diagram showing the number of open diffraction channels, Λ, depending on frequency ω and Bloch wave vector k_z.

the electric field $\mathbf{E}$ of eigenmodes in a 1D periodic chain [see Fig. 1(a)] has the following form:

$$\mathbf{E}(r, \varphi, z, t) = \mathbf{U}^s_{m,k_z}(z, r)e^{-i\omega t \pm ik_z z \pm im\varphi}. \quad (1)$$

Here, m is the orbital angular momentum (OAM), k_z is the Bloch wave vector defined in the first Brillouin zone, and superscript s encodes the index of the photonic band. The sign $\pm$ reflects the degeneracy of the modes propagating in opposite directions along the array and rotating in clockwise/counterclockwise directions. Each mode with indices m and s has its own dispersion $\omega = \omega^s_m(k_z)$. The dispersion of the two lowest modes with $m = 0$ is shown in Fig. 1(b) with the red solid lines. The function $\mathbf{U}^s_{m,k_z}(r, z)$ is a periodic function of the variable z with a period L. Its expansion into the Fourier series can be written as follows:

$$\mathbf{U}^s_{m,k_z}(z, r) = \sum_n \mathbf{C}^s_{m,k_z,n}(r)e^{\frac{2\pi i n}{L}z}. \quad (2)$$

In the general case, each mode consists of near fields and outgoing cylindrical waves. Therefore, the Fourier coefficient has the following asymptotic far from the chain axis:

$$\mathbf{C}^s_{m,k_z,n}(r) \to \overline{\mathbf{C}}^s_{m,k_z,n}H^{(1)}_m(\alpha_n r) \text{ as } r \to \infty. \quad (3)$$

Here, $H^{(1)}_m$ are the Hankel functions and $\alpha_n = [(\omega/c)^2 - (k_z + 2\pi n/L)^2]^{1/2}$ is the radial component of the wave vector. Indices n numerate the diffraction channels. For open channels, α_n is real, and for the closed ones, α_n is imaginary. The number of open diffraction channels, Λ, depends only on ω and k_z [see Fig. 1(b)]. If the amplitudes of all open diffraction channels are zero, we have a BIC. In the case of $k_z < \omega/c < |k_z \pm 2\pi/L|$, only one diffraction channel is open [the yellow area in Fig. 1(b)] and the radiation losses are determined only by the zero-order Fourier coefficient $\mathbf{C}^s_{m,k_z,0}(r) = \langle \mathbf{U}^s_{m,k_z}(r, z)\rangle_z$. Here, $\langle\cdot\rangle_z$ implies integration over the period of the chain. The structures symmetric with respect to the transformation $z \to -z$ allow for the existence of antisymmetric solutions at the Γ point, i.e., the so-called *symmetry-protected* BIC. Protection by the symmetry means, for example, that a substrate without a large refractive index (i.e., not opening the additional diffraction channels) does not destroy the BIC in spite of breaking the rotational symmetry of the chain. In other cases, BICs are called *accidental* or off-Γ BIC.

B. Infinite chain

In the considered geometry, the variables z and r are not separable. Therefore, the eigenfunctions $\mathbf{U}^s_{m,k_z}(z, r)$ and dispersion of the modes can be found only numerically. Figure 2(a) shows the dispersion of three eigenmodes with OAM $m = 0, 1, 2$ calculated numerically using COMSOL MULTIPHYSICS. The parameters of the chain are listed in the caption of Fig. 1. Below the light line, the modes have no radiation losses. Above the light line, the modes are leaky due to emanation into the first open diffraction channel. The dispersion of the radiation losses characterized by $\gamma = \mathrm{Im}[\omega(k_z)]$ is shown in Fig. 2(b). One can see that γ remains constant in the Γ point for the modes with $m = 1, 2$. However, the radiation losses for the mode with $m = 0$ tend to zero quadratically with k_z in the vicinity of the Γ point. The dashed line is the approximation of the numerical results by quadratic function $\gamma(k_z) = 0.26(k_z L/\pi)^2$ in the vicinity of the Γ point. Therefore, the mode with $m = 0$ turns into the BIC in the Γ point. Therefore, the mode with $m = 0$ turns into the BIC in the Γ point. The statement that this state is symmetry protected immediately follows from the distribution of the electric field E_φ [see Fig. 2(c)]. It is antisymmetric with respect to the center plane of the disk, and therefore it vanishes after averaging over the unit cell.

The states with $m = 0$ differ qualitatively from the states with nonzero OAM. Indeed, polarizations of the modes with $m = 0$ is completely separable into transverse electric (TE) and transverse magnetic (TM). For TE modes, $\mathbf{E} = (0, E_\varphi, 0)$ and $\mathbf{H} = (H_r, 0, H_z)$, and, for TM modes, $\mathbf{E} = (E_r, 0, E_z)$ and $\mathbf{H} = (0, H_\varphi, 0)$. This classification remains valid even for finite chains. Below, in Sec. IV A, we will use this fact for selective excitation of the symmetry-protected BIC with $m = 0$ via near fields. The BIC with $m = 0$ shown in Fig. 2(a) can be classified as a TE mode. Polarization of the modes with nonzero OAM ($m \neq 0$) is hybrid and it is contributed by both TE and TM components. Moreover, it follows from Maxwell's equations that the parity of the TE and TM components for these states in the Γ point is always different [52]. Therefore, it is impossible to cancel the far field in both polarizations simultaneously using only the symmetry reasons. Thus, there are no symmetry-protected BICs with $m \neq 0$ in the Γ point of k space. However, the accidental

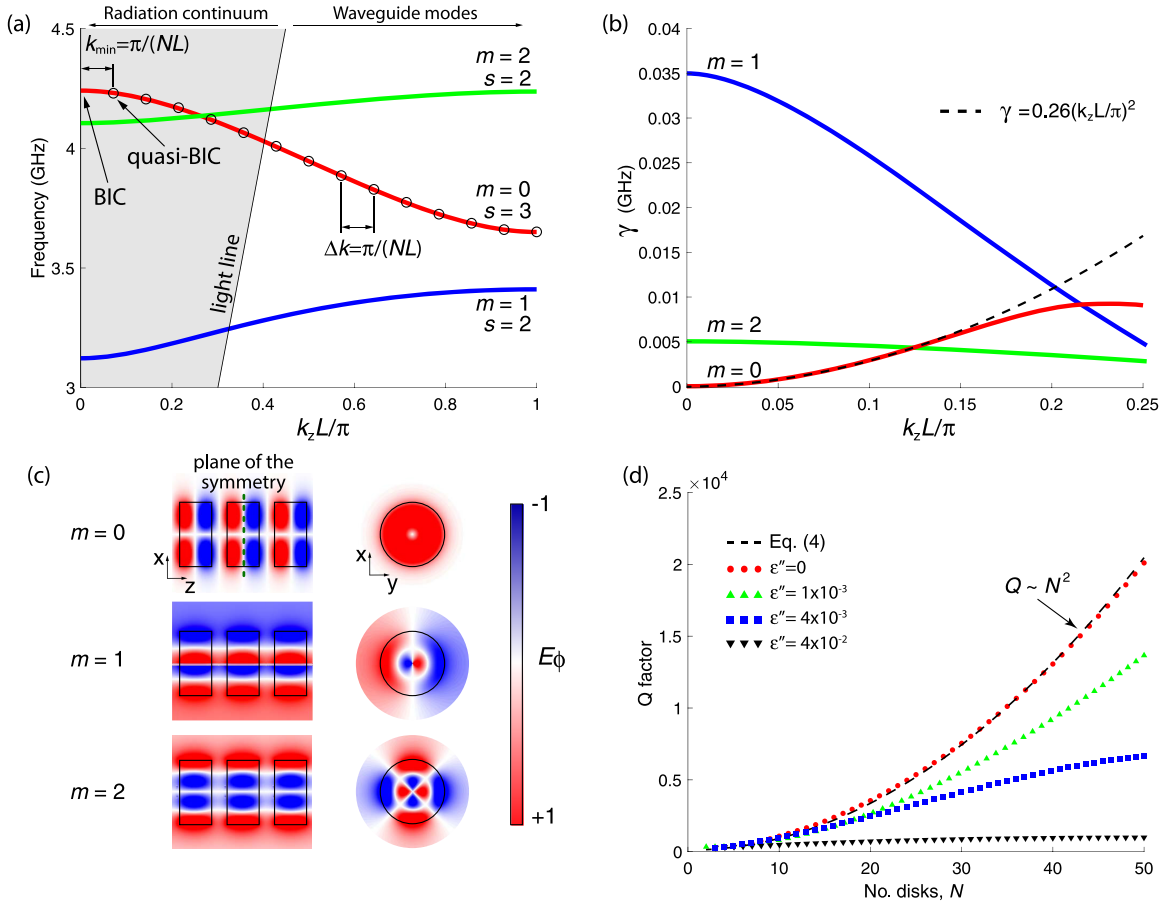

FIG. 2. (a) Dispersion of three eigenmodes with OAM $m = 0, 1, 2$ in the infinite chain of the ceramic disks. The Γ point for the mode with $m = 0$ corresponds to BIC. Index s shows the number of the photonic bands (see Appendix A for details). The parameters of the chain are mentioned in the caption of Fig. 1. The black circles show the dispersion of the eigenmode with $m = 0$ in a finite chain consisting of N periods. (b) Dispersion of the radiation losses for eigenmodes with OAM $m = 0, 1, 2$ in the infinite chain of the ceramic disks. The dashed line is the quadratic approximation of γ for $m = 0$. The approximation was made in the range $0 < k_zL/\pi < 0.1$ and then it was extrapolated to higher values of k_zL/π. (c) Side and front views of the distribution of the azimuthal electric field for the eigenmodes with OAM $m = 0, 1, 2$ at the Γ point. The upper row shows the field distribution for BIC. (d) Dependence of the Q factor for the number of periods in the chain for different levels of material losses obtained numerically using COMSOL MULTIPHYSICS. The dashed line is the quadratic approximation given by Eq. (4).

BIC in the Γ point can be obtained due to fine tuning of the geometrical or material parameters of the system [52].

C. Finite chain

In practice, we always deal with finite arrays of scatterers. Therefore, the diffraction continuum is not quantized completely and the diffraction channels are smeared, providing the radiation in the range of angles around diffraction directions of the infinite chain. Strictly speaking, this results in destruction of a true BIC, turning it into a quasi-BIC—a resonant state with high but finite value of Q factor.

The dependencies of the Q factor of quasi-BICs on the number of scatterers, N, for arrays of different dielectric particles have been studied theoretically for waveguide modes, leaky modes [53,54], and quasi-BIC [52,55–57]. In particular, it was predicted that the Q factor of the symmetry-protected BIC is proportional to N^2, while the Q factor of accidental BICs is proportional to N^3 [58]. Our simulations confirm that in the absence of material losses, the Q factor of the quasi-BIC at the Γ point grows as N^2 [Fig. 2(d)]. The experimental study of this dependence is provided is Sec. IV A.

The dependance of the Q factor on N can be obtained from the dependence of γ on k_z in the infinite chain [see the dashed line in Fig. 2(b)]. Indeed, photonic bands of a finite chain consist of a finite number of resonances placed equidistantly in the Brillouin zone. The distance between the neighbor resonances, $\Delta k_z = \pi/(NL)$, is defined by the Fabry-Perot quantization [Fig. 2(a)]. The resonance with the minimal Bloch wave vector $k_z^{\min} = \Delta k_z$ has the highest Q factor and this resonance can be associated with quasi-BIC as the closest state to the Γ point. Substitution of Δk_z into $\gamma(k_z)$ gives a simple estimation for the dependence of the Q factor of the quasi-BIC on the number of periods,

$$Q(k_z^{\min}) = \frac{\omega_{\mathrm{BIC}}}{2\gamma(\Delta k_z)} = \frac{4.24}{2 \cdot 0.26} N^2 \approx 8.15 N^2. \qquad (4)$$

This estimation agrees well with the results of the numerical simulation of the finite chains [see Fig. 2(d)]. This result means that radiation due to scattering on the ends of the chain is negligible.

Besides the radiation losses due to a finite size of the chain, there are other sources of losses (absorption in material, roughness of the scatterers, structure disorder, leakage into high-index substrate, etc.) which contribute to the total losses, even in the case of the infinite chain [52,55,59]. The practically important question is how many disks it is necessary to take to ensure that the radiation losses due to the finite size of the sample will be negligible with respect to other losses. Figure 2(d) shows the dependence of the Q factor of the quasi-BIC on the number of disks N for different levels of material losses introduced through the imaginary part of the permittivity ε''. For a larger number of the disks, the total Q factor saturates. It means that material losses give the main contribution into the total losses. The maximal achievable Q factor could be estimated as $Q_{\max} = \varepsilon'/\varepsilon''$.

III. SAMPLE

The sample represents a finite chain of the disks fabricated from a $BaO\text{-}TiO_2$ microwave ceramic placed equidistantly with the period $L = 15.1$ mm (see Fig. 1). The permittivity of the ceramics and tangent of losses extracted from the auxiliary experiment on measurement of the scattering cross section on a single ceramic disk in a microwave frequency band (2–5 GHz) are equal to $\varepsilon = 40.0$ and $\tan\delta = 2.5 \times 10^{-4}$, respectively (see Appendix B). The radius and the height of the disks are $R = 10.2$ and $h = 10.1$ mm, respectively. To fix the array, a special holder with grooves was fabricated from a Styrofoam material with a permittivity close to 1.1 at the microwave frequencies. Simple calculations show that the holder results in blueshift of the BIC with $m = 0$ at the Γ point less than 1 MHz and it does not affect the radiation losses at all since the BIC is symmetry protected.

The array of disks has two main advantages over the array of spheres. The first one is that disk resonators are easier to fabricate using a conventional sintering procedure of microwave ceramic powder after pressing it in a steel die. The second one is that disks have two scale parameters, height h and radius R. Their independent variation, together with the period of the chain L, allows one to provide precise mode engineering, getting a number of BICs with different orbital angular momenta and Bloch vectors [51].

It follows from Fig. 2 that the frequency bands for $m = 0$ and $m = 2$ overlap. This hinders the observation of the symmetry-protected BIC through measurement of the scattering cross section since the incident plane wave is contributed by cylindrical waves with all OAM. Thus, our preliminary experiments on measurement of the scattering cross section of the chain provided insufficient results because we cannot clearly distinguish the modes with $m = 2$ and quasi-BIC with $m = 0$ (see Appendix C).

IV. RESULTS OF MEASUREMENTS

A. Transmission spectra

As we mentioned above (see Sec. II B), the polarization of the mode with $m = 0$ is separated into TE and TM. Therefore, they can be selectively excited via near field by axially symmetric antennas placed coaxially with the chain. The TM modes can be excited by an electric dipole antenna, and the TE modes can be excited by a magnetic dipole antenna. Since the analyzed symmetry-protected BIC is a TE mode, in the experiment we use two identical shielded-loop antennas [60] placed coaxially with the chain and connected to ports of a vector network analyzer (VNA) [see Fig. 3(a)]. The antennas with the outer diameter of 10 mm have been fabricated from 086 semi-rigid coax cable. They are placed at the distance $D = 5$ mm away from the faces of the first and last disks. Such a distance provides a weak-coupling regime between the antennas that make the analysis of the Q factor of the quasi-BIC eligible (see Appendix D).

The measured transmission spectra of the array of 20 disks placed between two loop antennas are shown in Fig. 3(b). Two transmission bands consisting of 20 resonance peaks each are clearly seen. These bands correspond to the modes with $m = 0$ shown in Fig. 1(b). A weak ripple at frequencies 2.7–2.9 GHz correspond to the modes with $m = 1$, which are excited due to nonperfect axial symmetry of the sample. The resonances laying in the green area in Fig. 3(b) correspond to the waveguide modes of the infinite chain and the resonances

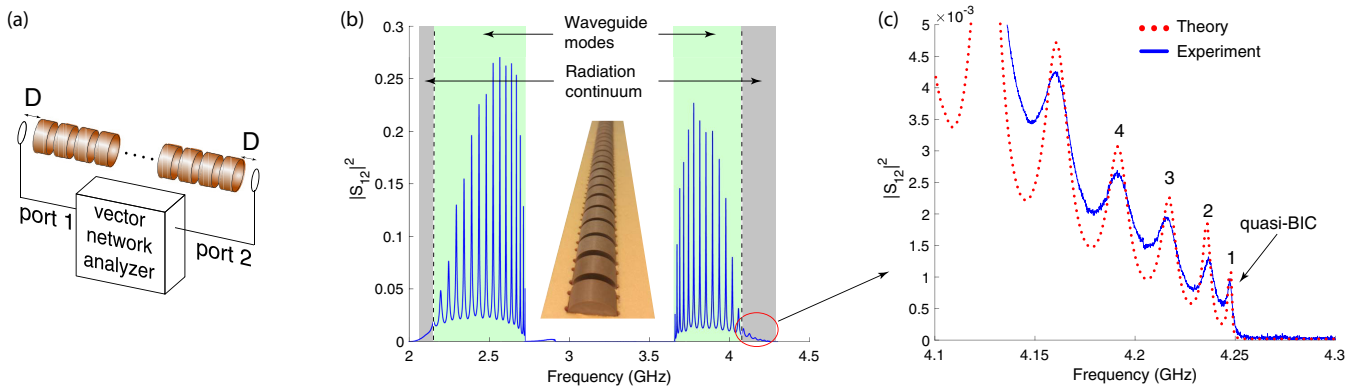

FIG. 3. (a) Artistic view of the experimental setup for measurement of the transmission spectra of the chain of the ceramics disks. (b) Experimental transmission spectra of the chain consisting of 20 ceramics disks placed between two coaxially positioned loop antennas. The parameters of the chain are shown in the caption of Fig. 1. The green and gray areas correspond to the waveguide and leaky modes, respectively. The inset shows the photo of the sample. (c) Zoomed-in view of the transmission spectra shown in (b). The dotted line shows the results of numerical simulations carried out in COMSOL MULTIPHYSICS. The last peak in the series corresponds to quasi-BIC.

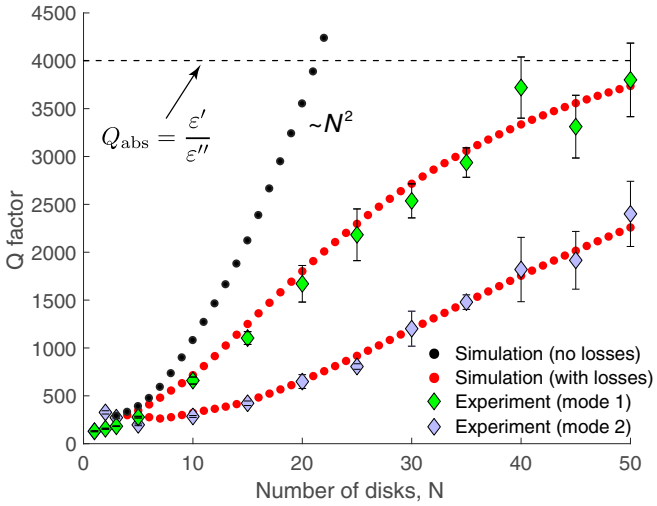

FIG. 4. Experimental dependence of Q factors of the symmetry-protected quasi-BIC (mode 1) and the neighboring resonance (mode 2) on the number of disks N in the chain of ceramics disks. Error bars indicate the standard deviation in the Q factor extracted from the transmission spectra measured five times. The parameters of the chain are mentioned in the caption of Fig. 1. The dotted line shows the results of numerical simulation in COMSOL MULTIPHYSICS.

in the gray area correspond to the leaky modes. The intensity of the leaky resonances in the transmission spectrum is very weak because of coupling with the continuum of radiation modes in surrounding space. Figure 3(b) shows the zoomed transmission spectra in the region of leaky modes. The blue solid line is the experimental data and the red dotted line is the result of numerical simulation carried out using COMSOL MULTIPHYSICS. Figure 3(c) shows clearly that the width of the last peak in the series is the most narrow. This peak corresponds to quasi-BIC, which transforms into a true BIC at the Γ point as $N \to \infty$. The amplitudes of the resonances in the transmission spectrum decrease approaching to the edge of the photonic band, and the amplitude of the peak corresponding to the quasi-BIC is minimal. It is explained by the decrease of the coupling between the loop antennas and the modes, when their$Q$ factor increases. Similar behavior is observed in the reflectance spectra of photonic crystal slabs supporting BICs [12].

Each transmission spectrum with a fixed number of disks was measured five times. After each measurement, the disks were extracted from the holder and shuffled. The experimental dependence of the Q factor for the two last resonances in the series [see mode 1 and mode 2 in Fig. 3(c)] on the number of the disks is shown in Fig. 4 by rhombus markers. The error bars show the standard deviation in the Q factors. The dotted lines correspond to the simulation. One can see that for small N, when the radiative losses are dominant, the Q factor increases quadratically. However, the deviation from the quadratic behavior becomes essential as $N \sim 20$. Further increase of the number of the disks results in saturation of the total Q factor to the level $Q_{abs} = \varepsilon'/\varepsilon''$. It is clear that the lower the material losses, the bigger the number of scatterers necessary to take in order to suppress the radiative losses of quasi-BIC with respect to the material absorption. The analyzed chain of the ceramic disks with $\tan\delta = 2.5 \times 10^{-4}$ behaves as an infinite one when the number of the disks is more than 50.

B. Field distribution

In the previous section, we analyzed the spectral characteristics of quasi-BIC. Here, we focus on the experimental study of its field profile. A true symmetry-protected BIC with $m = 0$ being the TE-polarized mode has only three nonzero components of electromagnetic field, E_φ, H_r, and H_z. It is notable that for the considered mode, the component H_r is not equal to zero only for the closed diffraction channel. Therefore, it characterizes only the structure of near fields. To measure the radial component of magnetic field H_r, we use the shielded-loop antenna as a probe [see Fig. 5(a)]. The antenna of the same geometry as the previous two has been connected to the third port of the VNA and fixed to an arm of a high-precision scanner equipped by an automated step motor. The magnetic field was probed at the distance of 1 mm above the disks along the array with the step of 0.5 mm. The frequency range to scan the magnetic field has been determined by the transmission coefficient measurement.

The measured magnetic field profiles for quasi-BIC and two neighbor resonances [see peaks 2 and 3 in Fig. 3(c)] for the chain of 20 disks are shown in Figs. 5(f)–5(h). The results of the numerical simulations carried out using COMSOL MULTIPHYSICS are shown in Figs. 5(b)–5(d). One can see that for the mode at $f = 4.249$ GHz, the envelope of the field profile is one-half of the sine period. Therefore, the observed mode is a symmetry-protected quasi-BIC with the minimal possible Bloch wave vector equal to $k_z = \pi/(LN)$.

V. TIGHT-BINDING MODEL

It is clearly seen from Fig. 3(b) that the transmission drops dramatically for resonances above the light line. It happens due to their coupling with the radiation continuum. This behavior could be described in the framework of the tight-binding approach accounting for the interaction between the neighbor disks and their coupling to the radiation continuum. The use of the tight-binding approach is natural because the ceramics disks composing the chain have a permittivity $\varepsilon = 40$ that makes the field well localized inside the disks [see Figs. 2(c) and 5(e)].

The tight-binding Hamiltonian of the chain consisting of N disks has $2N$ nodes coupled by an alternating way as shown in Fig. 6 [61]:

$$\widehat{H}_B = \sum_{j=1}^{2N} |\psi_j|^2 - \sum_{j=1}^{2N-1} u_j \psi_j \psi_{j+1}^* + \text{H.c.} \qquad (5)$$

Therefore, each disk is described by a pair of nodes with coupling coefficient u_1. Two nodes per disk are needed to realize an antisymmetric mode of the disk resulting in the appearance of BIC in the chain. The coupling between the disks is described by coefficient u_2. The effective Hamiltonian accounting for radiation losses and coupling with antennas

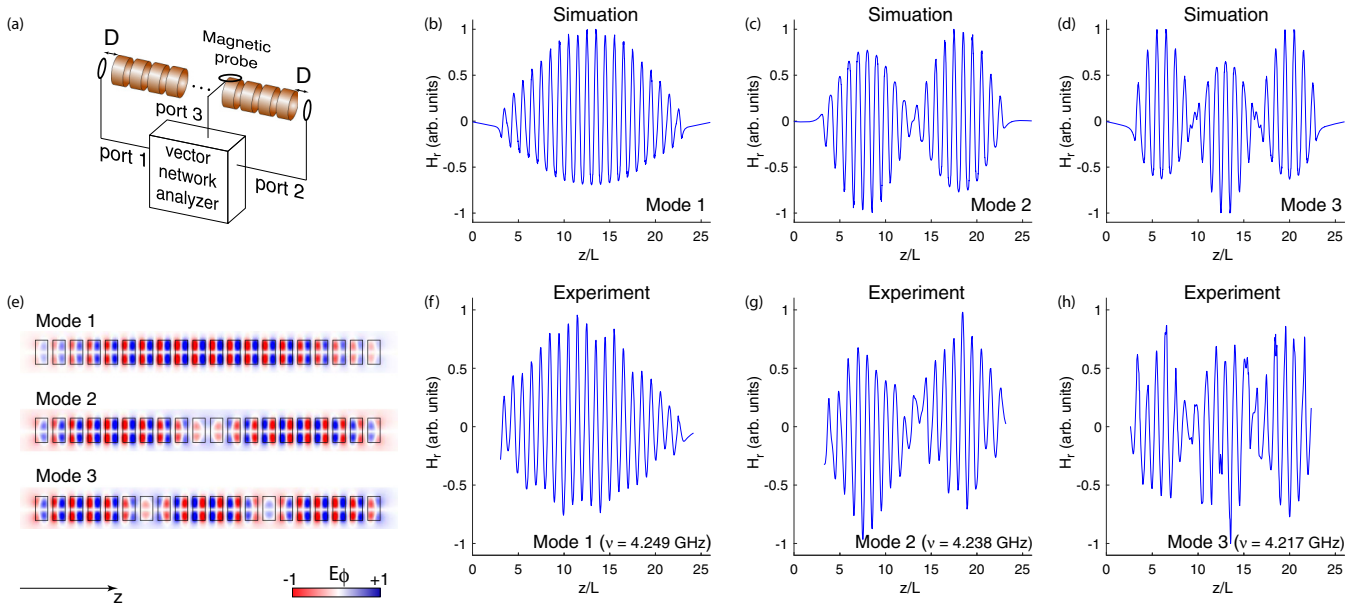

FIG. 5. (a) Artistic view setup for measurement of the distribution of the radial magnetic field component. (b)–(d) Numerically obtained distribution of the radial magnetic field component for the chain consisting of 20 ceramics disk. (e) Numerically obtained distribution of the azimuthal electric field component for the chain consisting of 20 ceramics disk. (f)–(h) Measured distribution of the radial magnetic field component for the chain consisting of 20 ceramic disks.

can be written as follows:

$$\widehat{H}_{\text{eff}} = \widehat{H}_B - \sum_{j=1}^{2N} [v_{aL} e^{ik} \delta_{j,1} + v_{aR} e^{ik} \delta_{j,2N} + v_{\text{rad}} e^{ik_p}]. \quad (6)$$

Here, the coefficients v_{aL} and v_{aR} are responsible for coupling with transmitting and receiving antennas, respectively, with the propagation band

$$E = 4 \sin^2 k. \quad (7)$$

The coefficient v_{rad} is responsible for coupling with the radiation continuum, which could be considered as a wide waveguide coupled to the array along its entire length. In order that only a part of the eigenvalues was embedded into the radiation continuum, we shift the cutoff energy of the radiation continuum separating the spectra of leaky and waveguide modes to the level $E = 3$,

$$E = 3 + 8 \sin^2 k_p. \quad (8)$$

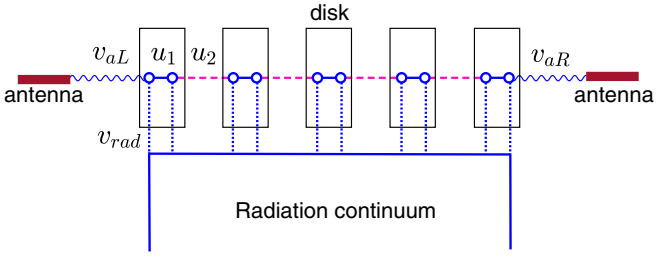

FIG. 6. The tight-binding simulation of the N disks coupled with the left and right antennas via the couplings v_{aL} and v_{aR}. The whole chain is coupled with the wide waveguide simulating the radiation continuum via the coupling v_{rad}.

The reference transmission spectrum for $N = 10$ calculated neglecting the coupling with the radiation continuum ($v_{\text{rad}} = 0$) is shown in Fig. 7(a). The used parameters are listed in the caption. One can see that the spectrum consists of the acousticlike and optical-like bands, which agrees with the experimental data [see Fig. 3(b)]. By analogy with the classification of phonon bands in solid-state physics, we imply that for the acousticlike band, wave functions ψ_j and ψ_{j+1} inside each of the disks are in-phase in the Γ point. For the optical-like band, the wave functions inside each of the disks are antiphase in the Γ point. The transmission at the resonances is close to unit. Introduction of the coupling ($v_{\text{rad}} \neq 0$) with the radiation continuum only affects the modes with energies above the cutoff [Fig. 7(b)]. The coupling to the continuum results in a leakage of the pumped wave from the left antenna into the radiation continuum and, respectively, a decrease of the transmission peaks at resonances energies above embedded into the radiation continuum. The following increase of v_{rad} results in blurring of the transmission peaks. The considered toy model well describes the experimental behavior of the transmission shown in Figs. 3(b) and 3(c).

VI. CONCLUSION

In this paper, we have observed a symmetry-protected bound state in the continuum (BIC) in the linear array of periodically arranged ceramic disks. In the experiment, we selectively excited the modes with zero orbital angular momentum by coaxially placed loop antennas and measured the transmission spectra of the array. We analyzed the dependence of the Q factor of the BIC on the number of disks in the chain and estimated the critical number of the disks making the radiation losses become negligible with respect to the material absorption. For the considered ceramics with tangent of losses

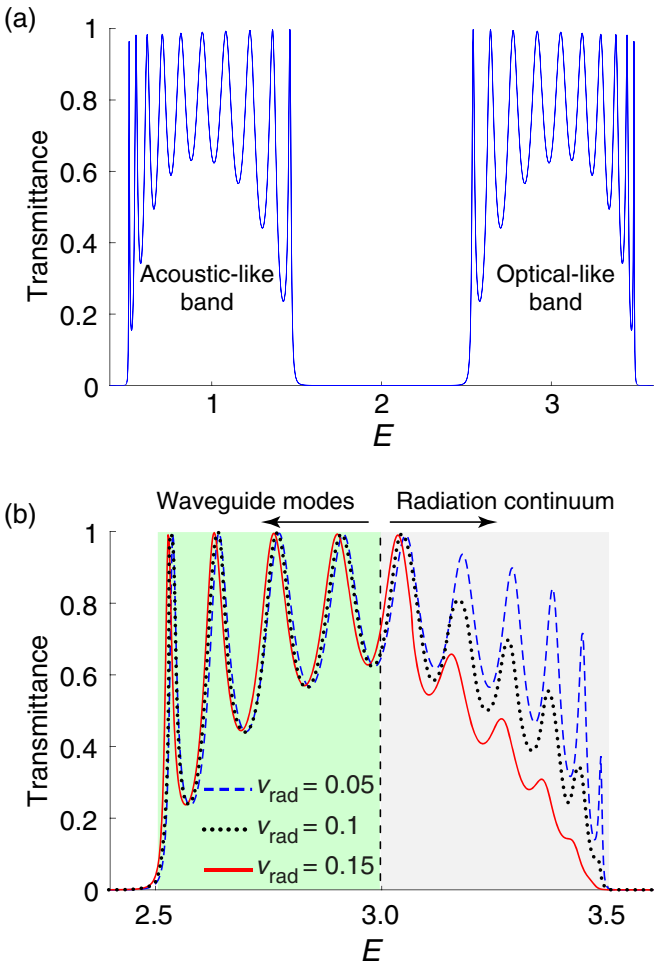

FIG. 7. The transmission spectra of the tight-binding model for (a) $v_{\rm rad} = 0$ and (b) $v_{\rm rad} \neq 0$, $u_1 = 0.5$, $u_2 = 1$, $v_{aL} = 0.5$, $v_{aR} = 0.6$.

$\tan\delta = 2.5 \times 10^{-4}$, this critical number of disks is about 50. We confirmed the observation of BIC by the measurements of the magnetic field profiles. All measurements are in a good agreement with the results of the numerical simulation and analytical model based on the tight-binding approximation. The obtained results provide useful guidelines for practical implementations of structures with bound states in the continuum, which opens up horizons for the development of optical and radio-frequency metadevices.

ACKNOWLEDGMENTS

The numerical simulations and experimental part of this work were supported by the Russian Science Foundation (Grant No. 17-12-01581), and the analytical calculations were supported by RFBR (Grant No. 18-32-20205) and the Ministry of Education and Science of the Russian Federation (3.1668.2017/4.6). The authors are thankful to Andrey Sayanskiy for assistance in the holder fabrication. A.A.B. and Z.F.S. acknowledge the Foundation for the Advancement of Theoretical Physics and Mathematics "BASIS" for valuable financial support.

Z.F.S. and M.A.B. contributed equally to this work.

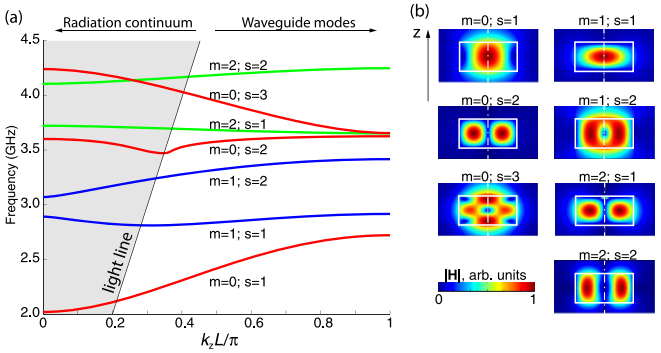

FIG. 8. (a) Dispersion of eigenmodes with OAM $m = 0, 1, 2$ in the infinite chain of the ceramic disks. (b) Calculated distribution of the magnetic field amplitude $|\mathbf{H}|$ of eigenmodes in a single ceramic cylinder.

APPENDIX A: BAND DIAGRAM

Figure 8(a) shows the calculated dispersion of eigenmodes with OAM $m = 0, 1, 2$. The photonic bands in the chain of cylinders are formed due to splitting of the eigenmodes of a single resonator. The calculated distributions of the magnetic field amplitude $|\mathbf{H}|$ of eigenmodes in a single ceramic cylinder are shown in Fig. 8(b).

APPENDIX B: ABSORPTION IN CERAMICS

To define the loss tangent of the ceramics, we measured the spectrum of the extinction cross section of a single ceramic disk in the vicinity of high-Q resonance, where absorption makes the dominant contribution to the total losses [see Fig. 9(a)]. To perform the measurements, the ceramic disk was placed in the middle between two wideband horn antennas. The antennae were connected to the ports of a vector network analyzer (VNA). The polarization of the incident wave is shown in the inset of Fig. 9(a). The spectrum of the extinction

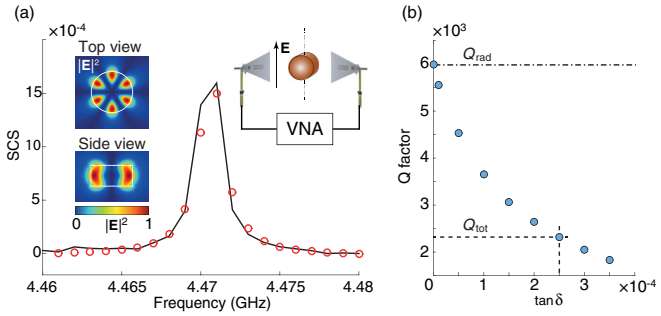

FIG. 9. (a) Measured extinction cross section of a single ceramic disk. The resonance corresponds to the mode with orbital angular momentum (OAM) $m = 3$. The left inset shows the distribution of $|\mathbf{E}|^2$ (top and side views). The right inset shows the scheme of the experiment. The solid line is the experimental data and the circle markers show the approximation. (b) Calculated dependence of the total Q factor for the resonance with $m = 3$ at $\omega_0 = 4.47$ GHz on the loss tangent. The dash-dotted line shows the Q factor in the absence of material losses in ceramics. The dashed lines correspond to the experimentally measured loss tangent $\tan\delta \approx 2.5 \times 10^{-4}$.

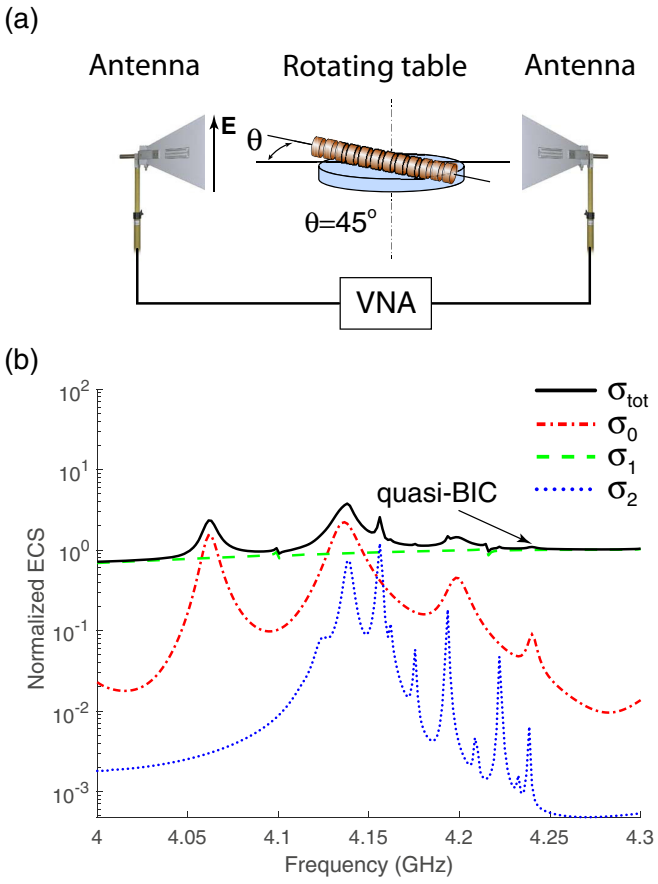

FIG. 10. (a) The scheme of the experiment on the measurement of the extinction cross section of the chain. (b) Calculated spectra of the total and partial extinction cross sections (ECSs) corresponding to OAM $m = 0, 1, 2$.

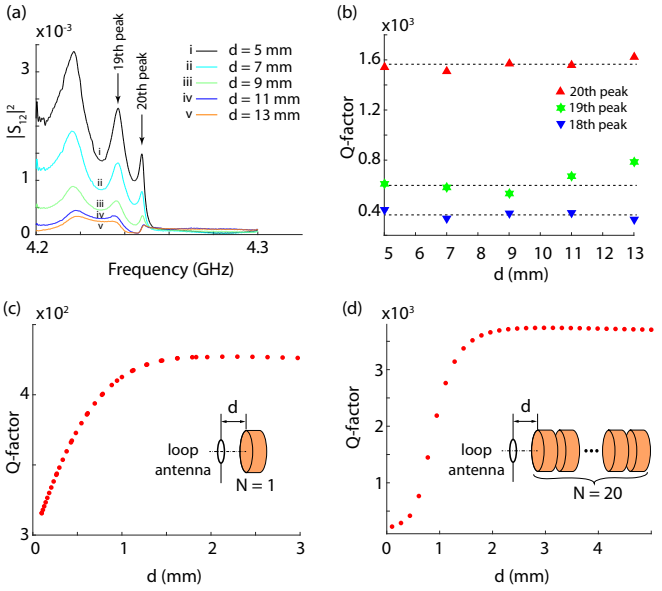

FIG. 11. (a) Transmission spectra $|S_{12}|^2$ of the chain consisting of 20 ceramic disks placed between two coaxially positioned loop antennas measured for different distances d between the antennas and the outermost disks. The parameters of the chain are shown in the caption of Fig. 1 of the main text. (b) Measured dependences of the Q factor of the last three resonances of the transmission band depending on the distance d between the antennas and the chain. (c) Numerically calculated dependence of the Q factor of the resonance with OAM $m = 2$ at the frequency 3.86 GHz in a single disk on the distance d between the disk and the loop antenna. (d) Numerically calculated dependence of the Q factor of the quasi-BIC (20th peak) in a chain consisting of 20 disks on the distance d between the outermost disk and the loop antenna. Material absorption in (c) and (d) are neglected.

cross section has been calculated by applying the optical theorem. Using the classical Fano formula [1],

$$F(\Omega) = A\frac{(\Omega + q)^2}{\Omega^2 + 1}, \tag{B1}$$

we extracted the Q factor of a resonance with the azimuthal number $m = 3$. Here, $\Omega = (\omega - \omega_0)/(\gamma/2)$ is a normalized frequency, ω_0 is the resonance frequency and γ is the damping constant of the mode, q is the Fano asymmetry parameter, and A is the amplitude of the resonance. The distribution of $|\mathbf{E}|^2$ for the resonance under consideration is shown in the inset of Fig. 9(a). The treatment of the experimental data yields the Q factor about 2.3×10^3. This is the total Q factor, which includes the radiation losses and losses due to absorption in the ceramics,

$$\frac{1}{Q_{\text{tot}}} = \frac{1}{Q_{\text{rad}}} + \frac{1}{Q_{\text{abs}}}. \tag{B2}$$

To find Q_{abs} from Eq. (B2), we obtain the Q_{rad} numerically using COMSOL MULTIPHYSICS software. The total Q factor of the analyzed mode equals 6×10^3. Substitution of this value to Eq. (B2) gives $Q_{\text{abs}} = 4 \times 10^3$. According to the definition, the loss tangent $\tan\delta = \varepsilon''/\varepsilon'$, and therefore $\tan\delta = 1/Q_{\text{abs}} = 2.5 \times 10^{-4}$. This value corresponds to $\varepsilon'' \approx 0.01$. We also find the dependence of Q_{tot} on $\tan\delta$ numerically using the eigensolver of COMSOL MULTIPHYSICS [see Fig. 9(b)]. The numerical calculations confirm that $\tan\delta = 2.5 \times 10^{-4}$ gives $Q_{\text{tot}} = 6 \times 10^3$ for the resonance at $\omega_0 = 4.47$ GHz. We used the found value of $\tan\delta$ to calculate the theoretical dependence of the total Q factors of the symmetry-protected quasi-BIC on the number of the disks in the array (see Fig. 4).

APPENDIX C: PLANE-WAVE SCATTERING FROM AN INFINITE CHAIN OF DISKS

A plane-wave incident on a chain of dielectric disks [see Fig. 10(a)] excites the modes with all OAM ($m = 0, 1, 2, \ldots$). For the considered design of the chain (see Fig. 1), the transmission bands corresponding to $m = 0$ and $m = 2$ overlap [see Fig. 2(a)]. Therefore, it is difficult to distinguish the resonances corresponding to the modes with $m = 0$ and $m = 2$ in the extinction spectra under a plane-wave excitation. Indeed, Fig. 10(b) shows the calculated spectra of partial extinction cross sections σ_m corresponding to $m = 0, 1, 2$ and the total extinction cross section σ_{tot} defined as their sum. It is worth mentioning that the modes with $m = 2$ appear in the transmission spectra if the loop antenna placed noncoaxially with the chain.

APPENDIX D: COUPLING STRENGTH BETWEEN DISK ARRAY AND LOOP ANTENNA

In the general case, the loop antenna used for the measurement of the transmission spectra of the disk chain makes an additional contribution into the losses of all resonances, particularly into the losses of quasi-BIC. To be sure that the additional losses arising due to the coupling of the antenna to the array are negligible, we provide additional experiments and numerical calculations.

Figure 11(a) shows the experimental transmission coefficient measured for different distances d between the array and antenna. Figure 11(b) shows that there is no dependence of Q factors of the last three resonances of the transmission band on d. This confirms indirectly that in the considered range of d, the coupling of the array to the antenna is weak and the antenna does not affect the Q factors of the resonances in the main text.

To be sure that we work in the weak-coupling regime not decreasing the radiation Q factor of quasi-BIC and other resonances, we provide a numerical simulation showing the dependence of the Q factor on d for a single disk and the array of 20 disks [see Figs. 11(c) and 11(d)]. Our calculations show that the antennas affect the Q factor of the resonances if d is less than about 1.5 mm. In the experiment (see Fig. 3), the distance d is 5 mm. Therefore, the measurements are provided in the weak-coupling regime.

[1] M. J. Adams, *An Introduction to Optical Waveguides* (Wiley, New York, 1981), Vol. 14.

[2] J. P. Torres and L. Torner, *Twisted Photons: Applications of Light with Orbital Angular Momentum* (Wiley, New York, 2011).

[3] S. G. Tikhodeev, N. A. Gippius, A. Christ, T. Zentgraf, J. Kuhl, and H. Giessen, Phys. Status Solidi C Conf. Ser. **2**, 795 (2005).

[4] A. L. Yablonskii, E. A. Muljarov, N. A. Gippius, S. G. Tikhodeev, T. Fujita, and T. Ishihara, J. Phys. Soc. Jpn. **70**, 1137 (2001).

[5] E. N. Bulgakov and A. F. Sadreev, Phys. Rev. A **90**, 053801 (2014).

[6] E. N. Bulgakov and A. F. Sadreev, Phys. Rev. A **92**, 023816 (2015).

[7] E. N. Bulgakov and D. N. Maksimov, Opt. Lett. **41**, 3888 (2016).

[8] J. von Neumann and E. Wigner, Phys. Z. **30**, 465 (1929).

[9] C. W. Hsu, B. Zhen, A. D. Stone, J. D. Joannopoulos, and M. Soljačić, Nat. Rev. Mater. **1**, 16048 (2016).

[10] S. P. Shipman and S. Venakides, Phys. Rev. E **71**, 026611 (2005).

[11] D. C. Marinica, A. G. Borisov, and S. V. Shabanov, Phys. Rev. Lett. **100**, 183902 (2008).

[12] C. W. Hsu, B. Zhen, J. Lee, S.-L. Chua, S. G. Johnson, J. D. Joannopoulos, and M. Soljačić, Nature (London) **499**, 188 (2013).

[13] S. Weimann, Y. Xu, R. Keil, A. E. Miroshnichenko, A. Tünnermann, S. Nolte, A. A. Sukhorukov, A. Szameit, and Y. S. Kivshar, Phys. Rev. Lett. **111**, 240403 (2013).

[14] C. W. Hsu, B. Zhen, S.-L. Chua, S. G. Johnson, J. D. Joannopoulos, and M. Soljačić, Light: Sci. Appl. **2**, e84 (2013).

[15] S. D. Krasikov, A. A. Bogdanov, and I. V. Iorsh, Phys. Rev. B **97**, 224309 (2018).

[16] Y. Yang, C. Peng, Y. Liang, Z. Li, and S. Noda, Phys. Rev. Lett. **113**, 037401 (2014).

[17] Z. Hu and Y. Y. Lu, J. Opt. **17**, 065601 (2015).

[18] M. Song, H. Yu, C. Wang, N. Yao, M. Pu, J. Luo, Z. Zhang, and X. Luo, Opt. Express **23**, 2895 (2015).

[19] C.-L. Zou, J.-M. Cui, F.-W. Sun, X. Xiong, X.-B. Zou, Z.-F. Han, and G.-C. Guo, Laser Photon. Rev. **9**, 114 (2015).

[20] Z. Wang, H. Zhang, L. Ni, W. Hu, and C. Peng, IEEE J. Quantum Electron. **52**, 6100109 (2016).

[21] L. Yuan and Y. Y. Lu, J. Phys. B **50**, 05LT01 (2017).

[22] J. Lee, B. Zhen, S.-L. Chua, W. Qiu, J. D. Joannopoulos, M. Soljačić, and O. Shapira, Phys. Rev. Lett. **109**, 067401 (2012).

[23] L. Li and H. Yin, Sci. Rep. **6**, 26988 (2016).

[24] Z. F. Sadrieva and A. A. Bogdanov, J. Phys. Conf. Ser. **741**, 012122 (2016).

[25] L. Ni, Z. Wang, C. Peng, and Z. Li, Phys. Rev. B **94**, 245148 (2016).

[26] Y. Wang, J. Song, L. Dong, and M. Lu, J. Opt. Soc. Amer. B **33**, 2472 (2016).

[27] X. Gao, C. W. Hsu, B. Zhen, X. Lin, J. D. Joannopoulos, M. Soljačić, and H. Chen, Sci. Rep. **6**, 31908 (2016).

[28] C. Blanchard, J.-P. Hugonin, and C. Sauvan, Phys. Rev. B **94**, 155303 (2016).

[29] K. Koshelev, S. Lepeshov, M. Liu, A. Bogdanov, and Y. Kivshar, Phys. Rev. Lett. **121**, 193903 (2018).

[30] R. Magnusson and S. Wang, Appl. Phys. Lett. **61**, 1022 (1992).

[31] M. Zhang and X. Zhang, Sci. Rep. **5**, 8266 (2015).

[32] V. Mocella and S. Romano, Phys. Rev. B **92**, 155117 (2015).

[33] J. W. Yoon, S. H. Song, and R. Magnusson, Sci. Rep. **5**, 18301 (2015).

[34] A. Kodigala, T. Lepetit, Q. Gu, B. Bahari, Y. Fainman, and B. Kanté, Nature (London) **541**, 196 (2017).

[35] B. Bahari, F. Vallini, T. Lepetit, R. Tellez-Limon, J. H. Park, A. Kodigala, Y. Fainman, and B. Kante, arXiv:1707.00181.

[36] J. M. Foley, S. M. Young, and J. D. Phillips, Phys. Rev. B **89**, 165111 (2014).

[37] X. Cui, H. Tian, Y. Du, G. Shi, and Z. Zhou, Sci. Rep. **6**, 36066 (2016).

[38] S. Romano, G. Zito, S. Torino, G. Calafiore, E. Penzo, G. Coppola, S. Cabrini, I. Rendina, and V. Mocella, Photonics Res. **6**, 726 (2018).

[39] Y. Liu, W. Zhou, and Y. Sun, Sensors **17**, 1861 (2017).

[40] K. L. Koshelev, S. K. Sychev, Z. F. Sadrieva, A. A. Bogdanov, and I. V. Iorsh, Phys. Rev. B **98**, 161113(R) (2018).

[41] H. M. Doeleman, F. Monticone, W. den Hollander, A. Alù, and A. F. Koenderink, Nat. Photon. **12**, 397 (2018).

[42] Y. Zhang, A. Chen, W. Liu, C. W. Hsu, B. Wang, F. Guan, X. Liu, L. Shi, L. Lu, and J. Zi, Phys. Rev. Lett. **120**, 186103 (2018).

[43] M. V. Rybin, K. L. Koshelev, Z. F. Sadrieva, K. B. Samusev, A. A. Bogdanov, M. F. Limonov, and Y. S. Kivshar, Phys. Rev. Lett. **119**, 243901 (2017).

[44] A. A. Bogdanov, K. L. Koshelev, P. V. Kapitanova, M. V. Rybin, and S. A. Gladyshev, Adv. Photon. **1**, 016001 (2019).
[45] K. Koshelev, G. Favraud, A. Bogdanov, Y. Kivshar, and A. Fratalocchi, Nanophotonics (2019), doi:10.1515/nanoph-2019-0024.
[46] K. Koshelev, A. Bogdanov, and Y. Kivshar, Sci. Bull. (2018), doi: 10.1016/j.scib.2018.12.003.
[47] W. Chen, Y. Chen, and W. Liu, arXiv:1808.05539.
[48] Z. Hu and Y. Y. Lu, J. Opt. Soc. Amer. B **34**, 1878 (2017).
[49] M. Padgett and R. Bowman, Nat. Photon. **5**, 343 (2011).
[50] A. M. Yao and M. J. Padgett, Adv. Opt. Photon. **3**, 161 (2011).
[51] E. N. Bulgakov and A. F. Sadreev, Phys. Rev. A **96**, 013841 (2017).
[52] E. Bulgakov and A. Sadreev, Adv. Electromagnet. **6**, 1 (2017).
[53] G. S. Blaustein, M. I. Gozman, O. Samoylova, I. Y. Polishchuk, and A. L. Burin, Opt. Express **15**, 17380 (2007).
[54] I. Y. Polishchuk, A. A. Anastasiev, E. A. Tsyvkunova, M. I. Gozman, S. V. Solovov, and Y. I. Polishchuk, Phys. Rev. A **95**, 053847 (2017).
[55] L. Ni, J. Jin, C. Peng, and Z. Li, Opt. Express **25**, 5580 (2017).
[56] E. N. Bulgakov and D. N. Maksimov, Opt. Express **25**, 14134 (2017).
[57] A. Taghizadeh and I.-S. Chung, Appl. Phys. Lett. **111**, 031114 (2017).
[58] E. N. Bulgakov and A. F. Sadreev, Phys. Rev. A **99**, 033851 (2019).
[59] Z. F. Sadrieva, I. S. Sinev, K. L. Koshelev, A. Samusev, I. V. Iorsh, O. Takayama, R. Malureanu, A. A. Bogdanov, and A. V. Lavrinenko, ACS Photon. **4**, 723 (2017).
[60] H. Whiteside and R. King, IEEE T. Antenna Propag. **12**, 291 (1964).
[61] A. F. Sadreev and I. Rotter, J. Phys. A **36**, 11413 (2003).